*G. Ausias[1] *, G. Dolo[1,2], D. Cartié[2], F. Challois[2], P. Joyot[3], J. Férec[1]*

[1] *Univ. Bretagne Sud, UMR CNRS 6027, IRDL, Lorient, France*
[2] *Coriolis Composites Technologies, Quéven, France*
[3] *ESTIA Recherche Technopole Izarbel, Bidart, France*

Modeling and Numerical Simulation of Laminated Thermoplastic Composites Manufactured by Laser-Assisted Automatic Tape Placement

A comprehensive numerical model is developed for the simulation of the laser-assisted automated tape placement process of carbon fiber/thermoplastic composites. After being heated with a laser, the thermoplastic is welded with the help of a consolidation roller onto a substrate made up of layers of tapes bonded onto one another. Under the pressure applied by the roller, the thermoplastic flows and the tape reaches its final thickness. The numerical model is developed in three sequential steps that can be used to identify the required pressure and temperature distribution to achieve a good bond. Firstly, a heat transfer simulation is performed to determine the temperature distribution into the incoming tape under the consolidation roller. Secondly, a rheological model is developed to examine the polymer flow under the roller and to obtain the pressure field. Finally, the consolidation level between the substrate and the tape is investigated through the degree of intimate contact, which is related to the processing parameters such as the roller velocity, the laser power density and the compaction force.

1 Introduction

Thermoplastics are a family of materials undergoing development for various reasons including recycling potential. They can be reinforced with discontinuous fibers but this technique is not optimal as the fiber orientation distribution induced by the process is not well controlled. Therefore, reinforcement with continuous fibers, as also encountered in thermoset composites, is more complex because the fiber impregnation by thermoplastics at molten state is difficult to achieve. Hence, tapes made with continuous fibers embedded in a thermoplastic resin are very attractive semi-finished products and easy to process. These tapes are automatically deposited layer-by-layer onto a substrate to manufacture engineering parts with reduced weight and optimal performance. This additive manufacturing technique is called Automated Fiber Placement (AFP) and its key point is to ensure a good consolidation between the different layers. The welding process consists in firstly heating the tape with a hot gas torch or a laser beam before applying a compaction force using a consolidation roller (Grouve et al., 2012). However, the complete consolidation of the part is solely guaranteed by a final consolidation stage under controlled pressure and temperature in an autoclave, which is the main weakness of this process. Thus, one of the major objectives is to remove this crucial step, which is time and energy consuming, in order to perform an in-situ consolidation directly at the layup stage. Manufacturing without the autoclave stage would allow the direct production of very large components such as a full fuselage section. This can be achieved only if the process is well controlled and if the consolidation state can be estimated after the heating step and the compaction by the roller.

Most applications using the AFP technology are dedicated to the aeronautics and aerospace industries and involve high-tech materials. One of the most used materials is the APC-2-PEEK thermoplastic polymer supplied by the Solvay group and is composed of 60 % by weight of continuous carbon fibers embedded in a PEEK – poly (ether-ether-ketone) – resin. This technical material can be used in highly loaded applications at temperatures up to 260 °C due its semi-crystalline nature and possesses excellent environmental resistance and toughness, and fire resistant properties. In some cases the thermoplastic matrix can also be made of PPS (Polyphenylene sulphide) (Grouve et al., 2013). This technology can also be used for dry fibers placement in RTM process (Belhaj et al., 2013) or for thermoset tape placement (Beakou et al., 2011; Lukaszewicz et al., 2012).

The AFP technology has great potential for applications to efficiently manufacture large composite structures and therefore, optimizing this process remains an open challenge (Esposito et al., 2019). However, uncertainties persist concerning the mechanical performances and physical properties of the final part, which are associated with the defects created by the process (Croft et al., 2011). Khan et al. (2013) performed a parametric study and concluded that a definition of optimized placement equipment is hard to provide. Due to the high vis-

* Mail address: Gilles Ausias, Univ. Bretagne Sud, UMR CNRS 6027, IRDL, F-56100 Lorient, France
E-mail: gilles.ausias@univ-ubs.fr

cosity of thermoplastics, continuous fibers move with the resin rather than relative to the resin. Resin flow through a fixed fiber network is the conventional process modeling method for autoclave thermoset processing due to the low viscosity of the thermosets prior to cure initiation. However, the suitable approach for thermoplastic composite consolidation is to consider a squeezing flow, where fibers are advected by the overall flow. Experimental observations on a unidirectional laminate showed that transverse squeeze flow is the prominent mechanism (Rogers, 1989). Ranganathan et al. (1995) developed a consolidation model based on a Newtonian viscous fluid for three specific cases (e. g.; isothermal incompressible, isothermal compressible and non-isothermal compressible) and were able to investigate the void reduction during the thermoplastic composites processing. Wang and Gutowski (1991) considered that the transverse flow can be described by the equations governing the flow of a power law fluid. Tierney and Gillespie (2006) computed the pressure and the temperature fields under the roller and then determined the quality of bonding between layers using the degree of intimate contact. Shuler and Advani (1996) examined experimentally the influence of the fiber volume fraction on the transverse shear viscosity of unidirectional composites (e. g.; APC-2) and found that their rheological behaviors are adequately predicted by a modified Carreau viscous model with a temperature dependence which followed an Arrhenius relationship. More recently, Barasinski et al. (2014) studied the thermal properties of the ply interfaces during in-situ consolidation. Finally, Chinesta et al. (2014), and then Argerich et al. (2018) developed the first steps of an advanced simulation of composites manufacturing for AFP based on proper generalized decompositions. As for Aized and Shirinzadeh (2011), they attempted to optimize a robotic fiber placement process with the objective of maximizing the product quality and the production rate.

Assembling APC-2 tapes requires heating the material to around 400 °C and, therefore, powerful heating systems are necessary. A hot air torch was the first device used for thermoplastic composites. This technique was applied for filament winding process with speeds of up to 0.05 m/s. Its main disadvantages are its reaction time, its low energy efficiency and the heating of surrounding tools. Furthermore, the hot air facilitates the oxidation reactions of the thermoplastic and then requires the use of an inert gas (Rizzolo and Walczyk, 2016). Later on, Beyeler and Guceri (1988) employed a 80 W CO_2 laser beam with a wavelength of 10.6 µm and a circular spot. In order to create a rectangular spot to homogeneously heat the tapes throughout their width, a system based on ZeSe lenses has been developed. Then, the use of a CO_2 laser is reported in a few publications (Funck and Neitzel 1995; Pistor et al., 1999; Rosselli et al., 1997). Nowadays, diode lasers dominate the market due to their higher energy efficiency, their life expectancy and the relatively easy integration of the device onto the machine using optical fiber to bring the energy from the power source to the placement head. They emit in the near infrared and can generate an energy density higher than the one provided by hot air torches (Comer et al., 2015). The ability of the laser to heat the composite depends on the absorption and reflectivity of the material (Le Louët et al., 2017). This high energy density must be well controlled as the process window is quite narrow between poor bond quality (too low heating energy) and thermoplastic matrix degradation (too high heating energy) (Dolo et al., 2017; Martín et al., 2018).

Since the consolidation between the tape and the substrate arises from chemical bonds at the interface, these interfacial bonds connecting adjacent plies are critical to the load-transfer efficiency (Leon et al., 2018). To understand how this bond between layers can be achieved, Comer et al. (2015) well summarized the different physical phenomena involved in layer bonding: (i) heating of the incoming tape and substrate material above the melting point, (ii) consolidation between them under temperature and pressure imposed by the roller, (iii) diffusion of polymer chains across the interface, and (iv) crystal formation and growth upon cooling. Modeling the formation of interfacial bonds can be viewed as a two-step approach: first intimate contact, then auto adhesion (Lee and Springer, 1987). Tape roughness is a key point to model two surfaces bonding together (Leon et al., 2016; Saoudi et al., 2017). Loos and Li (2000) described the tape roughness as rectangles of varying size to characterize the intimate contact between two layers. Then, Lee and Springer (1987) simplified the method by considering rectangles of an identical size and introduced a dependence with the pressure and the temperature. Mantell and Springer (1992) enhanced the expression for the degree of intimate contact by varying the applied pressure with position and time whereas the Newtonian viscosity is assumed to be temperature independent. More investigations on the tape roughness were performed by Yang and Pitchumani (2001; 2002b), who introduced effective fractal surfaces. Finally, the evolution of the non-isothermal degree of healing with time is given by Yang and Pitchumani (2002a).

To the knowledge of the authors, a non-isothermal process model for consolidation considering a Carreau fluid is not available in the literature. Furthermore, the estimation for the degree of intimate contact based on this model, with varying the applied pressure and taking into account a viscosity with position and temperature dependence, has not been proposed. So, the aim of this work is to fulfill this gap. In the present article, firstly, the characteristics of the investigated material are presented, and then a description of the AFP process with laser heating is given. Next, the theory of thermal analysis used to obtain the temperature field throughout the material during the process is summarized. Thus, a rheological model is proposed to describe the resin flow under the consolidation roller. Finally, the results are discussed and examined in terms of maximum temperature, force applied by the roller and degree of intimate contact.

2 Material and Process

2.1 Material

The raw material used in this work is a tape made of carbon fiber filled PEEK designated as APC-2. The matrix is a semi-crystalline thermoplastic PEEK polymer with a fusion temperature of 340 °C and a glass transition temperature of 143 °C (Diez-Pascual et al., 2012). Reinforcement is achieved by AS4 carbon fibers with an average diameter of 7 µm and a fiber volume fraction of about 60 %. The density of the composite at room temperature is 1 540 kg/m^3. This orthotropic material has

longitudinal (e. g.; in the direction parallel to the fiber axis) and transversal conductivities equal to 4.92 and 0.611 W/m/K, respectively, at 23 °C and equal to 7.68 and 0.658 W/m/K, respectively, at 400 °C (Kemmish et al., 2012). Linear interpolations are used between these values of conductivities. The specific heat is taken to be 1 425 J/kg/K.

The knowledge of the emissivity coefficient of the material is necessary to carry out thermal modeling. The emissivity of the APC-2 is measured using a FTIR spectrometer (model vertex v70, Bruker, France). A first transmission spectrum ensures that the material is opaque in the spectral range of 2 to 25 µm. The spectrometer is then combined with an integrating sphere A562 to determine the spectral reflectivity of the material. Integrations between 8 and 14 microns and between 2 and 25 µm finally give an emissivity coefficient ε equal to 0.864. For the infrared camera, emissivity coefficient ε is equal to 0.864 in its spectral range (8 to 14 µm).

The absorption coefficient of the APC-2 by the laser diode is obtained by comparing a numerical model with experimental results. The test consists of a static shooting with the laser over a period of 0.5 s and a power set to 400 W. Thermal modeling of the test is performed using 3D Abaqus software (Dassault Systemes, Vélizy-Villacoublay, France) finite element method. The calculation is divided into a heating stage followed by a cooling stage. Assuming the material is completely opaque, the intake of laser energy is considered as a surface flux.

Under the roller, the thermoplastic is supposed to be melted and the composite is considered to be a generalized Newtonian and transversely isotropic fluid. So, this high volume fraction aligned fiber composite exhibits different shear viscosities and elongational viscosities well defined by Pipes et al. (1994). They used micromechanics analysis and the hypothesis that fibers are parallel and uniformly distributed into the volume to give expressions for these viscosities. They are based on the matrix shear viscosity expressed using the Carreau model, which can be written as

$$\eta(\dot{\gamma}, T) = \bar{\eta}_0 \left[1 + \left(\bar{\lambda}\dot{\gamma}\right)^2\right]^{\frac{n-1}{2}}, \quad (1)$$

where $\bar{\eta}_0$ is the zero shear viscosity, $\bar{\lambda}$ is a constant related to the onset of shear thinning and n is the power-law exponent. The two first coefficients depend on temperature as proposed by Pipes et al. (1994) according to the following relations

$$\bar{\eta}_0 = a_T \eta_0, \quad \bar{\lambda} = a_T \lambda, \quad (2)$$

where

$$a_T = e^{\varsigma(T_0 - T)/T}, \quad (3)$$

ς is related to the activation energy of the viscosity, T is the temperature and T_0 is a reference temperature. The anisotropic rheological behavior of the composite is described by two axial viscosities and two elongational viscosities (Pipes et al., 1994). It is presumed that the flow motion under the roller is such that x is the flow direction and z is the shear direction. $\dot{\gamma}_{xz}$ is the associated shear rate. Pipes et al. (1994) expressed the composite viscosity using a factor κ which is the magnification of the fluid deformation rate caused by the presence of fibers. Thus, the shear viscosity of the composite can be written as

$$\eta_{xz}(\dot{\gamma}_{xz}, T) = \eta_0 a_T \kappa \left[1 + \left(a_T \kappa \lambda \dot{\gamma}_{xz}\right)^2\right]^{\frac{n-1}{2}}. \quad (4)$$

For APC-2, Pipes et al. (1994) also suggested the rheological coefficients which are summarized in Table 1. Plots of viscosity versus shear rate at different temperatures are depicted in Fig. 1. Shuler and Advani (1996) carried out a series of experiments on APC-2 and demonstrated that the model is relevant, which confirms the value of the rheological coefficients. More recently, Deignan et al. (2007) performed some rheological characterizations on this material and shown that its behavior is complex with notably a dependence on pressure.

2.2 Process and Experiments

The AFP technology developed by Coriolis Composites (Queven, France) consists in a poly-articulated robot extensively used in the automotive industry. This machine is equipped with a class 4 laser including diodes emitting in the near infrared with 2 wave lengths equal to 976 and 1025 nm, respectively. The radiation is delivered via an optical fiber to the head on which an optical system is installed for simultaneously heating the incoming tapes and the substrate, ensuring a good bond.

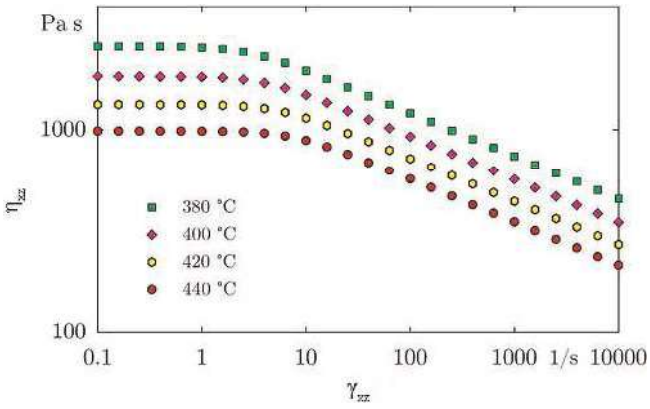

Fig. 1. Transverse shear viscosity versus shear rate for APC-2 at different temperatures

	η_0	λ	n	κ	ς	T_0
Unit	Pa s	s	–	–	–	°C
	280	0.038	0.787	6.69	11.07	399

Table 1. Rheological coefficients for APC-2 (Pipes et al., 1994)

The process consists of a ply-by-ply layup of composite tapes, with an initial cross section defined by its width $w_i = 6.35$ mm and its thickness $h_i = 0.15$ mm. The robot regulates the operational speed V of the head in the y-direction and the applied force F_C in the z-direction via the consolidation roller with a diameter of R = 68 mm. The x-direction corresponds to the tape width as depicted in Fig. 2. Laser heating is assumed to be uniform along the width of the tape and temperature distributions are found to be dependent on the x- and y-coordinates.

Due to the tape dimensions (i.e., its length is much larger than its width and thickness), the flow in the y-direction may be neglected and therefore the composite flow occurs in the (x, z) plane. The velocity is parallel to the x-direction, the gradient velocity is along the z-direction and the non-zero component of the pressure gradient is in the x-direction. This flow is induced by the roller compaction force, where the initial thickness h_i of the tape reduces to the final one h_f. Considering an incompressible material, the width w of the laid tape at the y-position can be easily determined. Locally, the squeezing velocity is denoted by $\dot{h}$ and a pressure field develops in the fluid. Thus, under temperature and pressure fields, bonding occurs between the tape and the substrate in the (x, y) plane located at z = 0. Once the two materials are in contact, consolidation starts and progresses as long as the pressure and temperature are sufficient. Consolidation evolution under the roller is evaluated thanks to the degree of intimate contact (see Section 6) computed along lines parallel to the y-direction. At the exit of the squeezing process (y = 0) the final degree of intimate contact will be depicted through the tape width.

3 Thermal Analysis

Since the entire structure for the AFP process is complex, thermal modeling is carried out by a finite element method in two dimensions (2D). Choosing a 2D simulation is justified by the small thickness of the tape as compared to its width (Chinesta et al., 2014) and by a uniform laser heating distribution through the width. The transient heat equation is solved in order to examine the effects of robot acceleration and deceleration as well as the edge effects. However, only results in a quasi-steady state are presented in this work. Toso et al. (2004) gave thermal boundary conditions for this problem. A free convection with a convection coefficient $h_{conv} = 13$ W/m^2/K is considered between the tape and the air, the latter being at room temperature. The radiation between the surfaces of the tape and its environment is also taken into account. The substrate is composed of 7 layers. Temperature exchanges with the toolings (e.g.; mold and consolidation roller) are described by convection with coefficients taken to be 709 W/m^2/K and 436 W/m^2/K, respectively. These values have been determined to well fit experimental data (Dolo 2017). The values of these convection coefficients are consistent according to data reported in Levy et al. (2014). The problem geometry is reduced to a simple rectangle in the case of a flat layup (i.e., the conveyed fibers are considered to be aligned along the rolling direction). The conveyed fibers are folded back onto the substrate to further simplify the geometry without perturbing the model, as done previously by Pitchumani et al. (1997). However, and in order to avoid heat exchange between the conveyed fibers and the substrate, an infinite thermal resistance is introduced at contact points upstream of the roller. The roller speed V and the laser power density P are assumed to be constant.

The lenses of the laser have been designed to light a rectangular window with an intensity profile close to a top-hat function. This allows to assume that the laser heating is uniform over the entire width of the tape, and therefore both the substrate and the conveyed tapes are heated with a uniform intensity.

Given the distribution of the laser radiation on the material, a thermal modeling is carried out at a macroscopic scale by considering homogeneous orthotropic properties for the composite. This development aims to find out the temperature field within the laminate, in particular as a function of the laser power density and the velocity of the layup, which are used to better understand and optimize the process.

4 Flow Modeling under the Consolidation Roller

4.1 Principle

Under the roller, the thickness of the tape decreases from the initial value of h_i at the primary contact point (located at $y = L_c$) to the final value h_f at y = 0 (see Fig. 2). L_c corresponds to the length of the squeezing area and h is the tape thickness at

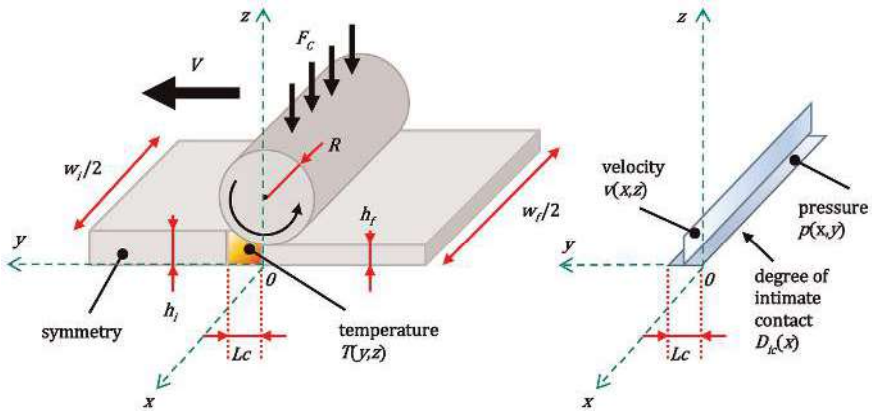

Fig. 2. Schematic representation of the consolidation process

the y-position. The squeezing velocity $\dot{h}$ is imposed by the roller. Since the material is presumed to be incompressible, the tape width w can be directly computed from the thickness. The polymer flow occurs in the (x, z) plane, shear rates change with the x- and z-coordinates and the viscosity can be expressed as $\eta_{xz}(x, z)$. The temperature distribution is found to be dependent on the x- and y-coordinates. The non-zero component of the pressure gradient is in the x-direction. In the area under the consolidation roller, the tape is supposed to be melted and subjected to a pressure p resulting from the force F_C applied by the roller. The head moves with a constant velocity V, which is controlled by the process. After being passed under the roller, the tape thickness is reduced to h_f and its width changes to w_f (see Fig. 2).

Note that in the (x-z) plane, temperatures and shear-rates depend on the position, therefore the local viscosity has to be considered as a function of the position such as $\eta \equiv \eta_{xz}(x, z)$. It results to solve a sequence of 2D squeeze flows in the (x-z) plane. Furthermore, the tape thickness is much smaller than its width leading to consider only the velocity gradient $\partial v_x/\partial z$ and its derivative with respect to the z-direction in the momentum equations.

The roller axis is parallel to the x-direction and is assumed to be cylindrical and rigid during the entire processing operation. Hence, from geometrical considerations, the contact length is found to be (Ranganathan et al., 1995)

$$L_c = \left[R^2 - (R - h_i + h_f)^2\right]^{1/2}. \tag{5}$$

Similarly, it is possible to express the imposed squeezing velocity as a function of the instantaneous height such as

$$\dot{h} = V\frac{\left[R^2 - (R - h_i + h_f)^2\right]^{1/2}}{(h_i - h_f - R)}. \tag{6}$$

Due to the symmetry of the problem in the x-direction, only half of the section is modeled.

4.2 Governing Equations

Fluid inertia effects are ignored due the high viscosity of the melted composite (low Reynolds number). Furthermore, body force terms are also omitted. With these assumptions in mind, the continuity and the momentum equations that govern the fluid motion can be written as

$$\frac{\partial v_x}{\partial x} + \frac{\partial v_z}{\partial z} = 0, \tag{7}$$

$$\frac{\partial p}{\partial x} = \frac{\partial}{\partial z}\left(\eta\frac{\partial v_x}{\partial z}\right), \tag{8}$$

$$\frac{\partial p}{\partial y} = \frac{\partial p}{\partial z} = 0. \tag{9}$$

According to Zheng et al. (2011), the fluidity S(x) is used to solve the momentum equation (Eq. 8) which results in (see Appendix A)

$$\bar{v}_x = \frac{S(x)}{h}\frac{\partial p}{\partial x}, \tag{10}$$

where $\bar{v}_x$ is the average velocity for the x-component through the instantaneous thickness of the tape, h. Note that the no-slip boundary conditions at the wall have been used and can be relaxed following the work of Ranganathan et al. (1995). The continuity equation (Eq. 7) can be arranged to give (see Appendix B)

$$\bar{v}_x = -\frac{\dot{h}}{h}x, \tag{11}$$

where $\dot{h}$ is the imposed squeezing velocity given in Eq. 6. Combining Eqs. 10 and 11 leads to

$$\frac{\partial p}{\partial x} = \frac{\dot{h}x}{S(x)}. \tag{12}$$

Considering the pressure to be equal to zero on the flow front (x = w/2), the pressure can be computed along the x axis. Once the pressure gradient is known, the x-component of the velocity can be determined with the following expression

$$v_x(x, z) = \frac{\partial p}{\partial x}\left[\int_0^z \frac{\xi}{\eta}d\xi - C(x)\int_0^z \frac{d\xi}{\eta}\right], \tag{13}$$

where C(x) is defined in Appendix A. The pressure field is obtained from integrating Eq. 13 by applying a zero pressure boundary condition on the surface at x = w/2. It results that

$$p(x) = \dot{h}\int_{w/2}^{x} \frac{xdx}{S(x)}. \tag{14}$$

It means that the flow front is not perturbed by the neighboring bands previously laid. Note that the pressure gradient is zero at x = 0 due to the symmetry of the problem. With the help of Zheng et al. (Zheng et al. 2011), the fluidity S(x) can be used and be defined as

$$S(x) = \int_0^h \frac{1}{\eta}\xi^2 d\xi - \frac{\left(\int_0^h \frac{1}{\eta}\xi d\xi\right)^2}{\int_0^h \frac{1}{\eta}d\xi}. \tag{15}$$

Finally, the velocity field can be expressed as

$$v_x(x, z) = \frac{dp}{dx}\left(\int_0^z \frac{1}{\eta}\xi d\xi - \frac{\int_0^h \frac{1}{\eta}\xi d\xi}{\int_0^h \frac{1}{\eta}d\xi}\int_0^z \frac{1}{\eta}d\xi\right). \tag{16}$$

5 Model Prediction

5.1 Numerical Implementation

The system of the governing equations is nonlinear and coupled, hence a known closed-form solution does not exist. Therefore, an iterative scheme is used to solve them. Near the area where the interface between the consolidation roller and the final tape height are very close (i.e., $h \approx h_f$ or $y \approx L_c$), the pressure gradients are very large and will cause numerical difficulties. A method of overcoming this problem is to use a variable mesh with the grid points clustered near the interface. The mesh in the (x-z) plane is a uniformly spaced grid in the computational domain.

It is therefore possible to calculate the thickness h at different y positions under the roller as well as the rate of thickness

decrease $\dot{h}$. The viscosity at each position (i.e., x and z) can be computed with the Carreau model using the local shear rate and temperature. Once the viscosity field is known, it can be used to evaluate the fluidity (Eq. 15) and then the pressure gradient, Eq. 11. Finally, Eq. 16 is used to determine the velocity field.

5.2 Simulation Results

It is recalled that 7 plies constitute the substrate and the 8th ply layup is modeled. The final tape thickness h_f is chosen equal to 0.12 mm and so the final width $w_f = 3.97$ mm and the contact length $L_c = 1.45$ mm is obtained from (Eq. 5). The relative thinning T_r is defined as the ratio of the final thickness to the initial thickness and is imposed to 0.8 in this first test. A numerical simulation has been carried out with a roller velocity of $V = 0.3$ m/s and a laser power density of $P = 200$ W/m^2. Firstly, a thermal analysis is carried out to compute the temperature field into the tape and the substrate. The temperature is mapped in the (y-z) plane and the maximum temperature is found to be 462 °C. Secondly the rheological simulation is performed. In Fig. 3, some velocity profiles are plotted at the location y = 1.002 mm, where the thickness is equal to 0.134 mm, and for 6 lateral positions (i.e., x = 0.528 mm, 1.131 mm, 1.735 mm, 2.338 mm, 2.942 mm and 3.545 mm, respectively). The greater the x position, the higher is the flow rate and the larger is the velocity profile. The analysis of the velocity profile shows that it is not exactly symmetrical along the vertical axis due the temperature gradient through the thickness. Note that on Fig. 3 the axis in the z-direction is expanded.

The pressure field is then computed in the (x-y) plane at z = 0, that is at the interface between the tape and the substrate under the roller. In this region, pressure and temperature contribute to achieve a good bond. Figure 4 represents the pressure field in the welding zone using iso-curves. The pressure reaches a high level and the maximum is on the symmetry line (x = 0) and is equal to 186.6 MPa. Tierney and Gillespie (2006) also got local pressure under the roller close to 200 MPa. In Fig. 4, the tape width is also drawn from the initial width at y = L_c to the maximum width at the exit of the welding area. Thus, the pressure can be integrated under the rolling area to get the compaction force F_c as

$$F_c = \int_0^{L_c} \int_0^{w(x)} p(x, y)dxdy. \quad (18)$$

The force was found to be 757 N and depends on the relative thinning and the roller velocity.

5.3 Abacus on Process Behavior

Several numerical simulations are then performed to propose an abacus relating the relative thinning, the compaction force and the roller velocity. They are carried out with a range of roller velocities between 0.3 m/s and 0.7 m/s and a range of laser power densities between 150 W/m^2 and 250 W/m^2. Relative thinning and final thickness are linked and both are represented on two vertical axes. For example, if the roller does not squeeze the tape, the final thickness remains at its initial value (i.e., $h_f = 0.15$ mm) and the relative thinning is equal to 1. As expected, the compaction force increases with the relative thinning and the roller velocity (see Fig. 5). For low velocities, the force required to get a small thickness (i.e., a large relative thinning) is reasonable. Hence, at 0.3 m/s a force of 757 N leads to a final thickness of 0.12 mm. However, when the speed increases, the force enhances very quickly and easily reaches the capabilities of the robot in terms of compaction force.

6 Consolidation

The aim of the laser and the roller is to produce both temperature and pressure fields that are high enough to bond the tape onto the substrate. Above the glass transition temperature, interdiffusion between the polymer surfaces occurs. The main stage in fusion bonding between two thermoplastic parts is the intimate contact process. It consists in the development of the interfacial contact region between the two materials. Intimate

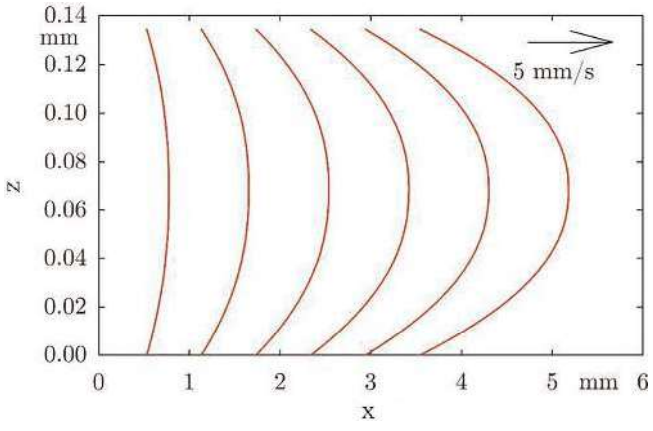

Fig. 3. Velocity profile through the thickness at y = 1.002 mm

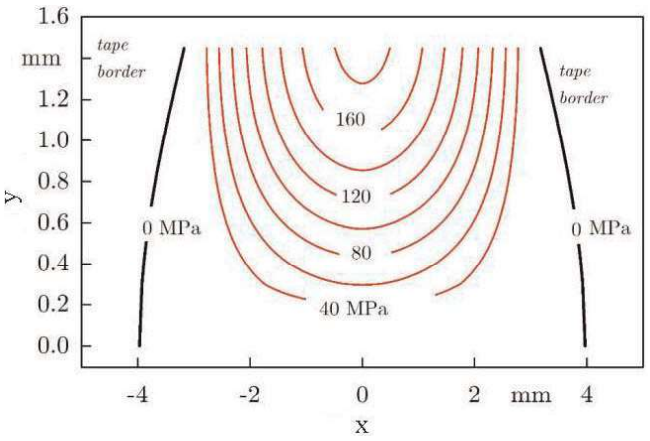

Fig. 4. Pressure field for a roller velocity of V = 0.3 m/s, a laser power density of P = 200 W/m^2 and a final thickness of h_f = 0.12 mm

contact is determined by the degree of intimate contact D_{ic} which can range from 0 for no bond to 1 for a perfect bond. The bond progresses when polymer chains diffuse across the interface. The pressure and the viscosity, which depend on the temperature, mainly control chain reptation at the interface. When the two surfaces are in contact, a sum of the ratio of pressure on viscosity is carried out for each time step. Mantell and Springer (1992) gave the following form to compute the degree of intimate contact

$$D_{ic} = a^* \left[\int_0^t \frac{p}{\eta_0(T)} d\tau \right]^{1/5}, \quad (19)$$

where $a^* = 0.29$ is the value assumed in this study and proposed by Pitchumani et al. (1996). $\eta_0(T)$ is the zero-shear viscosity depending on temperature and as already defined in Eq. 1. The welding occurs at the contact point between the tape and the substrate ($z = 0$). Numerical integration of D_{ic} is computed along a curve followed by the material of the tape under the roller at the interface between the tape and the substrate, and where the pressure is different from zero, i.e. $0 < y < L_c$. Figure 6 gives the profile of D_{ic} through the width of the tape after the compaction. A curve is plotted with the conditions set for the first simulation, for which the relative thinning is equal to 0.8. The pressure is maximum on the middle of the tape and decreases to zero on the tape border (Fig. 4) inducing a maximum of D_{ic} in the middle of the tape and a value equal to zero on the tape border, where the pressure is equal to zero. This is the reason why D_{ic} also decreases from a maximum on the center to zero on the edge of the tape.

Another simulation is carried out with a smaller final thickness of 0.10 mm and a relative thinning equal to 0.67. Figure 7 gives the pressure field which is higher compared to the first one (Fig. 4). In this case, the pressure undergone by the material is higher and the contact length increases as well. The pressure and temperature in the middle of the tape are large enough to get a D_{ic} equal to 1, meaning that a good bond is achieved (Fig. 6).

The set of numerical simulations carried out makes it possible to have a better understanding of the process operation and to obtain information on the temperature and pressure fields present at the core of the material. These quantities can then be used to determine the evolution of the material microstructure For instance, the material degradation (Dolo et al., 2017), the degree of crystallinity or the quality of the interlayer welding can be estimated from the history of the pressures and the temperatures undergone by each particle of matter. The maximum temperature is an important information to evaluate the risk of material degradation. An optimum is to be found between the need to heat the material to weld it correctly and the risk of degrading it. For each simulation, maxima of temperature and D_{ic} are computed versus laser power density and roller velocity in Fig. 8. Iso-curves are plotted and it can be noticed that they are mostly parallel, meaning that the maximum temperature and the maximum D_{ic} are strongly related.

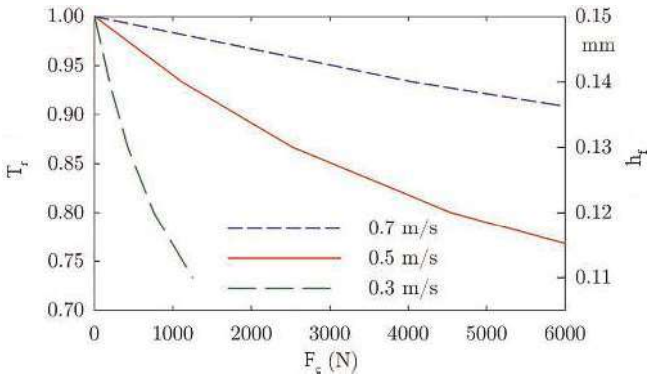

Fig. 5. Relative thinning versus compaction force for different roller velocities. The final thickness of the layup tape is also depicted

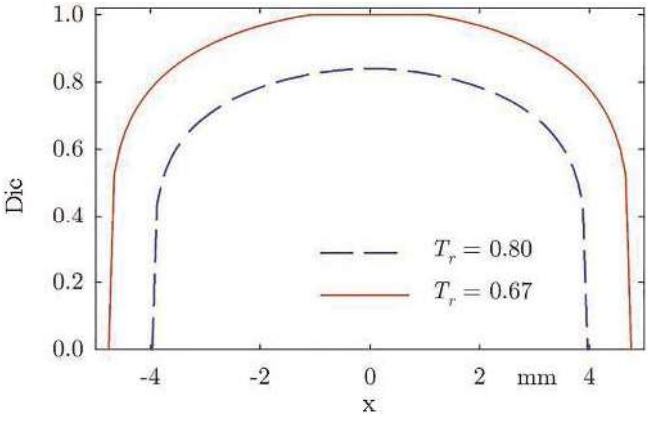

Fig. 6. D_{ic} through the width of the tape

7 Conclusion

A combined thermal-rheological model is presented for APC-2 composite processed with ATP process. A 2D thermal analysis is performed using a finite element method and validated with experimental works. Knowing the laser power input and the

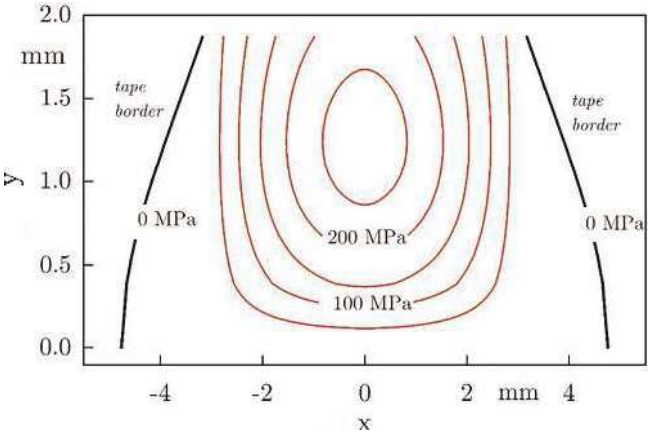

Fig. 7. Pressure field for a velocity of V = 0.3 m/s, a laser power density of P = 200 W/m² and a final thickness of h_f = 0.10 mm

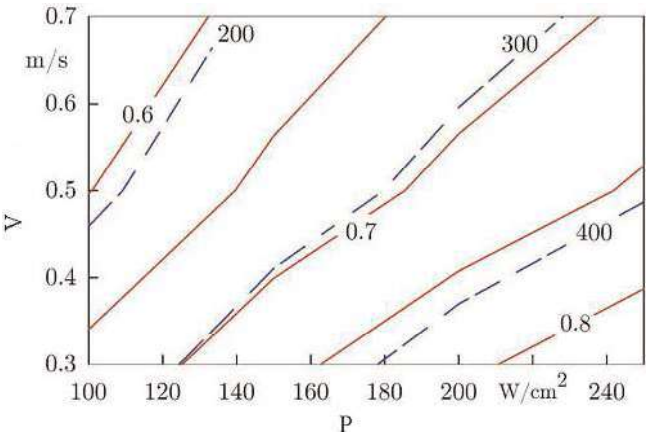

Fig. 8. D_{ic} (solid line) and temperature (dashed line) maxima versus laser power density and roller velocity for a relative thinning of 0.8

roller velocity, a temperature field is computed. Based on this first step, a rheological analysis of the flow under the compaction roller gives the velocity and pressure fields. The rheological behavior considers a Carreau model with a temperature dependence. Key points are relative thinning, roller speed and laser power. The pressure is straight used to compute the compaction force. Hence, an abacus gives the relation between the roller speed, the relative thinning and the laser power.

The control of the compaction force is relevant to get the required final thickness and finally the quality of the welding between layers. The quality of the bonding between the tape and substrate is determined by the degree of intimate contact, which depends on pressure and temperature at the interface. Once these two last parameters known, the model developed in this work is able to compute the degree of intimate contact through the width of the tape. This model could be very useful to control the process with a view to manufacturing parts in situ without post-processing.

References

Aized, T., Shirinzadeh, B., "Robotic Fiber Placement Process Analysis and Optimization Using Response Surface Method", Int. J. Adv. Manuf. Technol., **55**, 393–404 (2011), DOI:10.1007/s00170-010-3028-1

Argerich, C., Ibanez, R., Leon, A., Barasinski, A., Abisset-Chavanne, E. and Chinesta, F., "Tape Surface Characterization and Classification in Automated Tape Placement Processability: Modeling and Numerical Analysis", AIMS Materials Science, **5**, 870–888 (2018), DOI:10.3934/matersci.2018.5.870

Barasinski, A., Leygue, A., Soccard, E. and Poitou, A., "Identification of Non Uniform Thermal Contact Resistance in Automated Tape Placement Process", Int. J. Mater. Form., **7**, 479–486 (2014), DOI:10.1007/s12289-013-1144-9

Beakou, A., Cano, M., Le Cam, J. B. and Verney, V., "Modelling Slit Tape Buckling during Automated Prepreg Manufacturing: A Local Approach", Compos. Struct., **93**, 2628–2635 (2011), DOI:10.1016/j.compstruct.2011.04.030

Belhaj, M., Deleglise, M., Comas-Cardona, S., Demouveau, H., Binetruy, C., Duval, C. and Figueiredo, P., "Dry Fiber Automated Placement of Carbon Fibrous Preforms", Composites, Part B, **50**, 107–111 (2013), DOI:10.1016/j.compositesb.2013.01.014

Beyeler, E. P., Guceri, S. I., "Thermal Analysis of Laser Assisted Thermoplastic Matrix Composite Tape Consolidation", J. Heat Transfer, **110**, 424–430 (1988), DOI:10.1115/1.3250502

Chinesta, F., Leygue, A., Bognet, B., Ghnatios, C., Poulhaon, F., Bordeu, F., Barasinski, A., Poitou, A., Chatel, S. and Maison-Le-Poec, S., "First Steps towards an Advanced Simulation of Composites Manufacturing by Automated Tape Placement", Int. J. Mater. Form., **7**, 81–92 (2014), DOI:10.1007/s12289-012-1112-9

Comer, A. J., Ray, D., Obande, W. O., Jones, D., Lyons, J., Rosca, I., O'Higgins, R. M. and Mccarthy, M. A., "Mechanical Characterisation of Carbon Fibre-PEEK Manufactured by Laser-Assisted Automated-Tape-Placement and Autoclave", Composites, Part A, **69**, 10–20 (2015), DOI:10.1016/j.compositesa.2014.10.003

Croft, K., Lessard, L., Pasini, D., Hojjati, M., Chen, J. H. and Yousefpour, A., "Experimental Study of the Effect of Automated Fiber Placement Induced Defects on Performance of Composite Laminates", Composites, Part A, **42**, 484–491 (2011), DOI:10.1016/j.compositesa.2011.01.007

Deignan, A., Stanley, W. F. and Mccarthy, M. A., "Insights into Wide Variations in Carbon Fibre/Polyetheretherketone Rheology Data under Automated Tape Placement Processing Conditions", J. Compos. Mater., **52**, 2213–2228 (2018), DOI:10.1177/0021998317740733

Diez-Pascual, A. M., Naffakh, M., Marco, C., Ellis, G. and Gomez-Fatou, M. A., "High-Performance Nanocomposites Based on Polyetherketones", Prog. Mater. Sci., **57**, 1106–1190 (2012), DOI:10.1016/j.pmatsci.2012.03.003

Dolo, G., "Etude Expérimentale et Modélisation du Procédé de Placement de Fibres avec Chauffe Laser", Phd Thesis, Université Bretagne Sud, Lorient, France (2017)

Dolo, G., Férec, J., Cartié, D., Grohens, Y. and Ausias, G., "Model for Thermal Degradation of Carbon Fiber Filled Poly(ether ether ketone)", Polym. Degrad. Stab., **143**, 20–25 (2017), DOI:10.1016/j.polymdegradstab.2017.06.006

Esposito, L., Cutolo, A., Barile, M., Lecce, L., Mensitieri, G., Sacco, E. and Fraldi, M., "Topology Optimization-Guided Stiffening of Composites Realized through Automated Fiber Placement", Composites, Part B, **164**, 309–323 (2019), DOI:10.1016/j.compositesb.2018.11.032

Funck, R., Neitzel, M., "Improved Thermoplastic Tape Winding Using Laser or Direct-Flame Heating", Compos. Manuf., **6**, 189–192 (1995), DOI:10.1016/0956-7143(95)95010-V

Grouve, W. J. B., Warnet, L. L., Rietman, B. and Akkerman, R., "On the Weld Strength of in situ Tape Placed Reinforcements on Weave Reinforced Structures", Composites, Part A, **43**, 1530–1536 (2012), DOI:10.1016/j.compositesa.2012.04.010

Grouve, W. J. B., Warnet, L. L., Rietman, B., Visser, H. A. and Akkerman, R., "Optimization of the Tape Placement Process Parameters for Carbon-PPS Composites", Composites, Part A, **50**, 44–53 (2013), DOI:10.1016/j.compositesa.2013.03.003

Kemmish, D. J., Leach, D. C., "Poly(aryl ether ketone) Matrix Resins and Composites" in Wiley Encyclopedia of Composites, Nicolais, L., Borzacchiello, A. (Eds.), John Wiley & Sons, New Jersey, p. 1–20 (2012), DOI:10.1002/9781118097298.weoc171

Khan, M. A., Mitschang, P. and Schledjewski, R., "Parametric Study on Processing Parameters and Resulting Part Quality through Thermoplastic Tape Placement Process", J. Compos. Mater., **47**, 485–499 (2013), DOI:10.1177/0021998312441810

Le Louët, V., Rousseau, B., Le Corre, S., Boyard, N., Tardif, X., Delmas, J. and Delaunay, D., "Directional Spectral Reflectivity Measurements of a Carbon Fibre Reinforced Composite up to 450 °C", Int. J. Heat Mass Transfer, **112**, 882–890 (2017), DOI:10.1016/j.ijheatmasstransfer.2017.04.125

Lee, W. I., Springer, G. S., "A Model of the Manufacturing Process of Thermoplastic Matrix Composites", J. Compos. Mater., **21**, 1017–1055 (1987), DOI:10.1177/002199838702101103

Leon, A., Argerich, C., Barasinski, A., Soccard, E. and Chinesta, F., "Effects of Material and Process Parameters on in situ Consolidation", Int. J. Mater. Form., **12**, 491–503 (2018), DOI:10.1007/s12289-018-1430-7

Leon, A., Barasinski, A. and Chinesta, F., "Microstructural Analysis of Pre-Impreganted Tapes Consolidation", Int. J. Mate. Form., **10**, 369–378 (2016), DOI:10.1007/s12289-016-1285-8

Levy, A., Heider, D., Tierney, J. and Gillespie, J. W., "Inter-Layer Thermal Contact Resistance Evolution with the Degree of Intimate Contact in the Processing of Thermoplastic Composite Laminates", J. Compos. Mater., **48**, 491–503 (2014), DOI:10.1177/0021998313476318

Loos, A. C., Li, M. C., "Chapter 7 Consolidation during Thermoplastic Composite Processing" in, Processing of Composites, Davé, R. S., Loos, A. C. (Eds.), Hanser, Munich, p. 208–238 (2000), DOI:10.3139/9783446401778.007

Lukaszewicz, D., Ward, C. and Potter, K. D., "The Engineering Aspects of Automated Prepreg Layup: History, Present and Future", Composites, Part B, **43**, 997–1009 (2012), DOI:10.1016/j.compositesb.2011.12.003

Mantell, S. C., Springer, G. S.,"Manufacturing Process Models for Thermoplastic Composites", J. Compos. Mater., **26**, 2348–2377 (1992), DOI:10.1177/002199839202601602

Martín, M. I., Rodríguez-Lence, F., Güemes, A., Fernández-López, A., Pérez-Maqueda, L. A. and Perejón, A., "On the Determination of Thermal Degradation Effects and Detection Techniques for Thermoplastic Composites Obtained by Automatic Lamination", Composites, Part A, **111**, 23–32 (2018), DOI:10.1016/j.compositesa.2018.05.006

Pipes, R. B., Coffin, D. W., Simacek, P., Shuler, S. F. and Okine, R. K., "Chapter 4 Rheological Behavior of Collimated Fiber Thermoplastic Composite Materials" in Flow and Rheology in Polymer Composites Manufacturing, Advani, S. G. (Ed.), 10th Volume, Elsevier, Amsterdam, p. 85–125 (1994), DOI:10.1016/S0927-0108(97)80010-0

Pistor, C. M., Yardimci, M. A. and Guceri, S. I.,"On-Line Consolidation of Thermoplastic Composites Using Laser Scanning", Composites, Part A, **30**, 1149–1157 (1999), DOI:10.1016/S1359-835X(99)00030-5

Pitchumani, R., Gillespie, J. W. and Lamonta, M. A., "Design and Optimization of a Thermoplastic Tow-Placement Process with in situ Consolidation", J. Compos. Mater. **31**, 244–275 (1997), DOI:10.1177/002199839703100302

Pitchumani, R., Ranganathan, S., Don, R. C., Gillespie, M. A. and Lamonta, M. A.,"Analysis of Transport Phenomena Governing Interfacial Bonding and Void Dynamics during Thermoplastic Tow-Placement", Int. J. Heat Mass Transfer, **39**, 1883–1897 (1996), DOI:10.1016/0017-9310(95)00271-5

Ranganathan, S., Advani, S. G. and Lamontia, M. A., "A Nonisothermal Process Model for Consolidation and Void Reduction during in situ Tow Placement of Thermoplastic Composites", J. Compos. Mater., **29**, 1040–1062 (1995), DOI:10.1177/002199839502900803

Rizzolo, R. H., Walczyk, D. F., "Ultrasonic Consolidation of Thermoplastic Composite Prepreg for Automated Fiber Placement", J. Thermoplast. Compos. Mater., **29**, 1480–1497 (2016), DOI:10.1177/0892705714565705

Rogers, T. G., "Squeezing Flow of Fiber-Reinforced Viscous Fluids", J. Eng. Math., **23**, 81–89 (1989), DOI:10.1007/BF00058434

Rosselli, F., Santare, M. H. and Guceri, S. I., "Effects of Processing on Laser Assisted Thermoplastic Tape Consolidation", Composites, Part A, **28**, 1023–1033 (1997), DOI:10.1016/S1359-835X(97)00072-9

Saoudi, A., Leon, A., Grégoire, G., Barasinski, A., Djebaili, H. and Chinesta, F., "On the Interfacial Thermal Properties of Two Rough Surfaces in Contact in Preimpregnated Composites Consolidation", Surf. Topogr. Metrol. Prop., **5**, 045010 (2017), DOI:10.1088/2051-672X/aa9667

Shuler, S. F., Advani, S., "Transverse Squeeze Flow of Concentrated Aligned Fibers in Viscous Fluids", J. Non-Newtonian Fluid Mech., **65**, 47–74 (1996), DOI:10.1016/0377-0257(96)01440-1

Tierney, J., Gillespie, J. W., "Modeling of in situ Strength Development for the Thermoplastic Composite Tow Placement Process", J. Compos. Mater., **40**, 1487–1506 (2006), DOI:10.1177/0021998306060162

Toso, Y. M. P., Ermanni, P. and Poulikakos, D., "Thermal Phenomena in Fiber-Reinforced Thermoplastic Tape Winding Process: Computational Simulations and Experimental Validations", J. Compos. Mater., **38**, 107–135 (2004), DOI:10.1177/0021998304038651

Wang, E. L. and Gutowski, T. G., "Laps and Gaps in Thermoplastic Composites Processing", Composites Manufacturing, **2**, 69–77 (1991), DOI:10.1016/0956-7143(91)90182-G

Yang, F., Pitchumani, R.," Healing of Thermoplastic Polymers at an Interface under Nonisothermal Conditions", Macromolecules, **35**, 3213–3224 (2002a), DOI:10.1021/ma010858o

Yang, F., Pitchumani, R., "Interlaminar Contact Development during Thermoplastic Fusion Bonding", Polym. Eng. Sci., **42**, 424–438 (2002b), DOI:10.1002/pen.10960

Zheng, R., Tanner, R. I. and Fan, X.: Injection Molding – Integration of Theory and Modeling Methods, Springer, Berlin (2011), DOI:10.1007/978-3-642-21263-5

Acknowledgements

The authors would like to thank Y. Rageot, a Masters student at the Université Bretagne Sud for helping to develop numerical simulations.

Date received: April 16, 2020
Date accepted: July 14, 2020

Bibliography
DOI 10.3139/217.3976
Intern. Polymer Processing
XXXV (2020) 5; page 471–480

ISSN 0930-777X

Appendix A

The momentum equation (Eq. 8) is firstly integrated with respect to z from 0 to z and one obtains

$$\frac{\partial p}{\partial x} z = \eta \frac{dv_x}{dz} - A(x) \tag{A1}$$

where $A(x) = \eta \left.\frac{dv_x}{dz}\right|_{z=0}$ is constant for a given x. Dividing both sides of Eq. A1 by η and integrating again from 0 to z results, after some rearrangements, in

$$v_x = \frac{\partial p}{\partial x} \int_0^z \frac{1}{\eta} \xi d\xi + A(x) \int_0^z \frac{1}{\eta} d\xi \tag{A2}$$

where the no-slip boundary condition at z = 0 has been used for v_x. Applying once again the no-slip condition to Eq. A2, but this time at z = h, gives

$$A(x) = -\frac{\partial p}{\partial x} \frac{\int_0^z \frac{1}{\eta} \xi d\xi}{\int_0^z \frac{1}{\eta} d\xi} = -\frac{\partial p}{\partial x} C(x) \tag{A3}$$

where C(x) is a function of x such as

$$C(x) = \frac{\int_0^z \frac{1}{\eta} \xi d\xi}{\int_0^z \frac{1}{\eta} d\xi} \tag{A4}$$

The substitution of Eq. A3 into Eq. A2 yields

$$v_x = \frac{\partial p}{\partial x} \left[\int_0^z \frac{1}{\eta} \xi d\xi - C(x) \int_0^z \frac{1}{\eta} d\xi \right] \tag{A5}$$

Then, the average velocity $\bar{v}_x$ is introduced such as

$$\bar{v}_x = \frac{1}{h} \int_0^h v_x dz \tag{A6}$$

Therefore, inserting Eq. A5 into Eq. A6 leads to

$$\bar{v}_x = \frac{1}{h} \frac{\partial p}{\partial x} \left[\int_0^h \int_0^z \frac{1}{\eta} \xi d\xi dz - C(x) \int_0^h \int_0^z \frac{1}{\eta} d\xi dz \right] \tag{A7}$$

Both integrals appearing in Eq. A7 are evaluated using integration by parts resulting in the following expressions

$$\int_0^h \int_0^z \frac{1}{\eta} \xi d\xi dz = h \int_0^h \frac{1}{\eta} \xi d\xi - \int_0^h \frac{1}{\eta} \xi^2 d\xi \tag{A8}$$

and

$$\int_0^h \int_0^z \frac{1}{\eta} d\xi dz = h \int_0^h \frac{1}{\eta} d\xi - \int_0^h \frac{1}{\eta} \xi d\xi \tag{A9}$$

Substituting Eqs. A8 and A9 into Eq. A7 with the use of Eq. A3 gives

$$\bar{v}_x = -\frac{S(x)}{h} \frac{\partial p}{\partial x} \tag{A10}$$

where

$$S(x) = \int_0^h \frac{1}{\eta} \xi^2 d\xi - \frac{\left(\int_0^h \frac{1}{\eta} \xi d\xi \right)^2}{\int_0^h \frac{1}{\eta} d\xi} \tag{A11}$$

is the fluidity introduced by Zheng et al. (2011). Note that if the fluid is considered to be Newtonian, the fluidity becomes $S(x) = h^3/12\eta_0$, where η_0 represents the Newtonian viscosity.

Appendix B

To obtain Eq. 11, the continuity equation (Eq. 7) is integrated with respect to z from 0 to h to give

$$\frac{\partial}{\partial x} \int_0^h v_x dz + [v_z]_0^h = 0 \tag{B1}$$

By using the boundary conditions for v_z, that are $v_z(0) = 0$ and $v_z(h) = \dot{h}$, and noting that the average velocity for v_x defined in Eq. A6 appears in Eq. B1, one obtains

$$\frac{\partial}{\partial x} \bar{v}_x = \frac{\dot{h}}{h} \tag{B2}$$

A last integration gives

$$\bar{v}_x = \frac{\dot{h}}{h} x \tag{B3}$$

where the condition $\bar{v}_x = 0$ at x = 0 has been used.